Extreme internal solitary waves in the ocean: Theoretical considerations

K. G. Lamb

University of Waterloo, Waterloo, Ontario Canada

Abstract. Limiting forms of extreme internal solitary waves in the ocean are discussed from a theoretical standpoint. Exact solutions are compared with predictions of weakly nonlinear theory.

Introduction

Large amplitude internal solitary waves are frequently observed in coastal regions of the world's oceans where they are generated by the interaction of the barotropic tide with the shelf break. Waves with amplitude to depth ratios as large as 0.3 have been observed in the South China Sea (*Orr and Mignery* 2003) (70–m waves in 240 m depth) and off the Oregon coast (*Trevorrow* 1998) (22 m in 71 m depth). *Santon and Ostrovsky* (1998) observed internal solitary waves in a two-layer stratification off the Oregon coast which had amplitudes of 25 m in water 147 m deep. The amplitude to depth ratio is only about 0.17 in this case, however the wave amplitude was about 3.5 times larger than the thickness of the upper layer making them extremely nonlinear.

Internal solitary waves are important because they are often large, very energetic events, and, particularly in the coastal marine environment, they have a significant role in particle transport, mixing and energy dissipation, as well as affecting acoustic propagation. Understanding the impact of large internal solitary waves is of key importance in the coastal marine environment.

Here we review one approach for computing exact fully nonlinear internal solitary waves. Limiting forms of internal solitary waves are discussed. Next weakly nonlinear theory for internal waves, of the KdV type, are discussed with an emphasis on some of the shortcomings of this approach.

Exact internal solitary waves

A solitary wave is a wave of the form $F(x - Vt)$. That is, it propagates at constant speed without changing shape. For nonlinear dispersive waves, which is the case of interest here, solitary waves have special shapes, the shape depending on the governing evolution equation and the wave amplitude. We will only consider solitary waves with $F(\xi) \to 0$ as $\xi \to \pm\infty$.

Fully nonlinear, dispersive internal solitary waves can be computed by solving a nonlinear elliptic eigenvalue problem, the Dubreil-Jacotin-Long (DJL) equation, for the streamline displacement $\eta(x, z)$ or for the streamfunction (*Davis and Acrivos* 1967; *Tung, Chan and Kubota* 1982; *Turkington et al.* 1991; *Lamb and Wan* 1998; *Brown and Christie* 1998; *Stastna and Lamb* 2002).

Given the buoyancy frequency $N(z)$ where

$$N^2 = -g\bar{\rho}'(z)/\bar{\rho}(z), \tag{1}$$

and the background flow $\bar{U}(z)$ we need to solve

$$\begin{aligned}\nabla^2\eta + \frac{N^2(z-\eta)}{\big(c-\bar{U}(z-\eta)\big)^2}\,\eta \\ + \left(\frac{\bar{U}'(z-\eta)}{c-\bar{U}(z-\eta)} + \frac{N^2(z-\eta)}{2g}\right) \\ \times \left(\eta_x^2 + (1-\eta_z)^2 - 1\right) = 0,\end{aligned} \tag{2}$$

subject to the boundary conditions

$$\eta = 0 \text{ at } z = -H, 0 \quad \text{and} \quad \eta \to 0 \text{ as } x \to \pm\infty. \tag{3}$$

The propagation speed of the wave, c, is an eigenvalue which must be found as part of the solution.

The propagation speed of internal waves decreases as the mode-number increases and as the wave-length decreases. This makes it possible for internal solitary-like waves of mode-n > 1 to be accompanied by a wave train comprised of short, linear lower-mode dispersive waves with the same phase speed as the leading solitary-like wave. This generally seems to be the case (*Akylas and Grimshaw* 1992). Because the group velocity is smaller than the phase speed the dispersive wave train drains energy out of the solitary-like wave, resulting in a gradual decrease in the amplitude of the solitary-like wave. Thus exact internal solitary waves of mode greater than one do not exist except possibly under exceptional circumstances. One exception to this is for a stratification which is symmetric about the mid-depth for which symmetric mode-two solitary waves can be computed by calculating a mode-one wave in the upper half of the water column and reflecting the resulting wave about the mid-depth. This is often done in so-called studies of 'mode-two' waves (e.g. *Tung et al.* 1982). In addition, if a free surface is used, a dispersive wave train of short surface waves will radiate energy, implying that an exact internal solitary

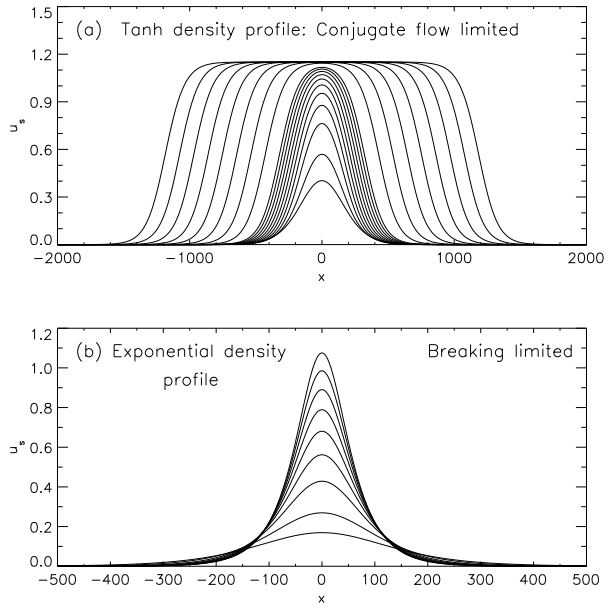

Figure 1. Horizontal velocity profiles along the surface for a sequency of internal solitary waves. Upper panel $\bar{\rho} = 1 - a(1 + \tanh(z/10)$. Lower panel: $\bar{\rho} = a + b \exp z/15$. The water depth is 100 m and a and b are chosen so the nondimensional density at the bottom is 1 and at the surface is 0.99.

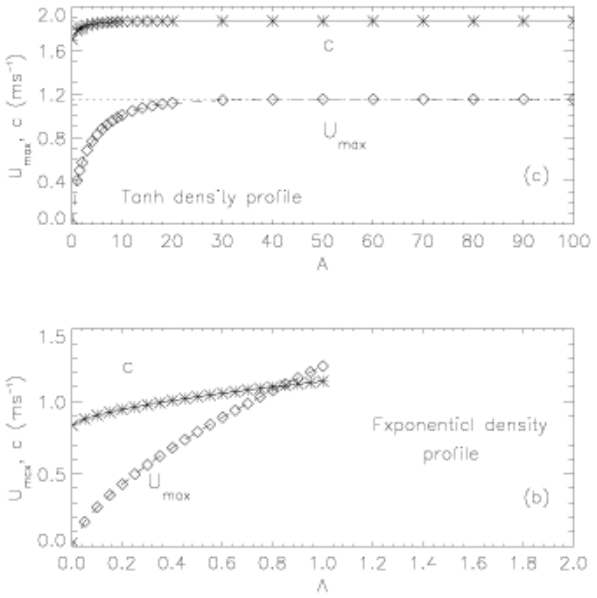

Figure 2. Propagation speeds and maximum horizontal current for solitary waves of increasing amplitude. Same density profiles as for Figure 1.

mode-one wave does not exist. While mode-one solitary-like waves with a free surface are easily generated in the laboratory, as are higher-mode internal solitary-like waves, only mathematically exact mode-1 solitary waves can be calculated and then only in the presence of a rigid lid.

In the following the Boussinesq approximation is made, simplifying the eigenvalue problem to

$$\nabla^2\eta + \frac{N^2(z-\eta)}{\big(c-\bar{U}(z-\eta)\big)^2}\,\eta + \left(\frac{\bar{U}'(z-\eta)}{c-\bar{U}(z-\eta)}\right)\big(\eta_x^2 + (1-\eta_z)^2 - 1\big) = 0. \tag{4}$$

In the absence of a background current the only nonlinearity is through the dependence of N^2 on $z - \eta$. If N is constant (linear stratification under the Boussinesq approximation) the equation is linear and no solitary wave solutions exist.

The solution method is based on the variational scheme developed by *Turkington et al.* (1991) which was extended to include background currents by *Stastna and Lamb* (2002). The solution $\eta(x, z)$ is the function which minimizes

$$K(\eta) = \int\int_R \frac{(\bar{U}(z-\eta)-c)^2}{2c^2}\Big[\eta_x^2 + (1-\eta_z)^2 + 1\Big]\,dx\,dz, \tag{5}$$

subject to the constraint that

$$F(\eta) = \int\int_R \int_0^\eta \Big(\bar{\rho}\big(z-\eta\big) - \bar{\rho}\big(z-s\big)\Big)\,ds\,dx\,dz, \tag{6}$$

takes on a specified value. Here $F(\eta)$ is the scaled available potential energy (APE) while $K(\eta)$ is the kinetic energy up to a constant if $\bar{U} = 0$. Thus, the wave amplitude is fixed by specifying the APE in the wave, a useful approach in computing broad waves.

Waves that can be computed are limited in one of three ways. First, as the APE is increased waves may flatten and broaden as the wave amplitude (maximum isopycnal displacement), propagation speed c and maximal horizontal current u_{max} all approach asymptotic limits with $u_{max} < c$. The flow in the central portion of such waves becomes horizontally uniform. This horizontally uniform flow is said to be conjugate to the upstream flow so we call this limit the conjugate flow limit. Observations of flat crested waves have been reported by (see page 18 of *Lafond* (1959)).

A second possibility is that as the wave amplitude increases u_{max} can reach and exceed c. When $u_{max} = c$ the wave is at the breaking limit. While waves beyond the breaking limit can be computed they have closed streamlines (i.e., a wave core, or vortex core) and the solution is no longer unique. Waves with cores have been observed in the lab (*Manasseh et al.* 1998; *Grue et al*. 2000), in the atmosphere (e.g., *Clarke et al*. 1981; *Cheung and Little* 1990)

and possibly in the ocean (Farmer, personal communication. See *Moum et al.* 2004). Internal solitary waves with core have been studied theoretically and numerically (*Derzho and Grimshaw* 1997; *Aigner et al*. 1999; *Lamb* 2002, 2003; *Lamb and Wilkie* 2004). Figure 1 shows some horizontal velocity profiles along the upper boundary $u(x,0)$ for a sequence of waves of increasing APE for an exponential density profile (maximum N at the surface) and for a hyperbolic tangent density profile with a well defined pycnocline at a depth of 30 m (total water depth 100 m). Figure 2 shows the propagation speed and maximum current u_{max} as a function of the scaled APE.

The third limiting mechanism is the onset of instability. The numerical method used to solve (4) uses an iterative solver which sometimes fails to converge. This appears to be related to the onset of an instability as typically the loss of convergence occurs when the minimum Richardson number in the pycnocline falls slightly below 0.25. This loss of convergence occurs even when one gradually increases the wave amplitude by computing a sequence of waves for increasing values of the APE.

Weakly nonlinear theory for long internal waves

Most theoretical descriptions of internal solitary waves are based on weakly nonlinear theory. In this approach the wave is assumed to be long relative to a vertical length scale, and of small amplitude. These imply that the waves are weakly dispersive and weakly nonlinear. Possible vertical length scales to which the wave length is compared could be the thickness of the upper mixed layer, or the total depth. The former leads to the Benjamin-Ono equation, the latter to the Korteweg-de Vries equation. Fully nonlinear, weakly dispersive evolution equations for internal waves have been developed (*Ostrovsky and Grue* 2003; *Craig et al*. 2004), however these are restricted to two-layer systems. These, together with the Benjamin-Ono equation, are not considered here.

The governing equations, nondimensionalized using horizontal and vertical length scales L (typical wavelength) and H (water depth), reference density ρ_o, time scale N_o^{-1} where N_o is a typical value of the buoyancy frequency, and horizontal velocity scale $U = HN_o$, are

$$\begin{aligned}\psi_{zzt} + U(z)\psi_{zzx} - U''(z)\psi_x - b_x \\ = \epsilon J(\psi,\psi_{zz}) - \mu(\psi_{xxt} + U(z)\psi_{xxx}) \\ + \epsilon\mu J(\psi,\psi_{xx}),\end{aligned} \tag{7}$$

$$\begin{aligned}b_t + U(z)b_x + N^2(z)\psi(x) \\ = \epsilon J(\Psi, b_z).\end{aligned} \tag{8}$$

Here $\epsilon\Psi$ and $\epsilon\rho$ are the perturbation streamfunction and density fields and $b = g\rho$. The derivation of the KdV equation is based on an expansion of Ψ and b in powers of the two small parameters ϵ, the wave amplitude, and $\mu = (H/L)^2$.

A search for solutions of the form

$$\psi = \psi^{(0)} + \epsilon\psi^{(1,0)} + \mu\psi^{(0,1)} + \epsilon^2\psi^{(2,0)} + \cdots, \tag{9}$$

$$b = b^{(0)} + \epsilon b^{(1,0)} + \mu b^{(0,1)} + \epsilon^2 b^{(2,0)} + \cdots, \tag{10}$$

for which each term is a separable function leads to a solution of the form

$$\psi = B(x,t)c\phi(z) + \epsilon B^2(x,t)c^2\phi^{(1,0)}(z) + \cdots, \tag{11}$$

$$\frac{b}{N^2} = B(x,t)E(z) + \epsilon B^2(x,t)E^{(1,0)}(z) + \cdots, \tag{12}$$

$$\zeta = B(x,t)Z(y) + B^2(x,t)Z^{(1,0)}(y) + \cdots. \tag{13}$$

where $\zeta(x,y,t)$ is the isopycnal displacement as a function of a vertical Lagrangian coordinate y.

At leading order we have

$$\mathcal{L}[\phi] \equiv \phi'' + \left(\frac{N^2}{(c-U)^2} + \frac{U''}{c-U}\right)\phi = 0, \tag{14}$$

$$\phi(-1) = \phi(0) = 0, \tag{15}$$

$$\tag{16}$$

and

$$Z = E = \frac{c}{c-U}\phi \tag{17}$$

is a solution of

$$\mathcal{M}[Z] \equiv \Big[(c-U)^2 Z'\Big]' + N^2(z)Z = 0. \tag{18}$$

These equations are eigenvalue problems for the separation constant c which is the linear long wave propagation speed. The wave amplitude function $B(x,t)$ satisfies

$$B_t + cB_x = 0, \tag{19}$$

to leading order. Separability of the higher-order terms requires that the evolution equation for B have higher-order terms. To order ϵ and μ, we obtain Korteweg-de Vries equation (KdV)

$$B_t + cB_x + \epsilon\alpha BB_x + \mu\beta B_{xxx} = 0. \tag{20}$$

The coefficients α and β are determined by solvability conditions for the higher order vertical structure functions. For example, the $O(\epsilon)$ vertical structure functions are determined by

$$\begin{aligned}\mathcal{L}[\phi^{(1,0)}] = \frac{\alpha}{c}\left(\frac{\phi''}{c-U} + \frac{U''}{(c-U)^2}\phi\right) \\ + \frac{3}{2}N^2\frac{U'}{(c-U)^4}\phi^2 + \left(\frac{U''}{c-U}\right)'\frac{\phi^2}{2(c-U)} \\ + \frac{(N^2)'}{(c-U)^3}\phi^2,\end{aligned} \tag{21}$$

$$\mathcal{M}[Z^{(1,0)}] = \alpha\Big[(c-U)Z'\Big]' + \frac{3}{2}\Big[(c-U)^2 Z'^2\Big]', \quad (22)$$

and

$$E^{(1,0)} = Z^{(1,0)} - ZZ' - \frac{1}{2}\frac{\left(N^2\right)'}{N^2}Z^2. \quad (23)$$

with homogeneous boundary conditions at $z = -1, 0$. Multiplying (21) by ϕ and integrating over the water column results in the left hand side being zero. Setting the right-hand side to zero then determines the value of α. Equivalently, equation (22) could be used by multiplying both sides by Z and integrating.

The equations for $\phi^{(1,0)}$ and $Z^{(1,0)}$ are forced versions of the equation for ϕ and Z. This implies that the solutions include an arbitrary multiple of the leading-order structure functions. If, for example, we define $Z_*^{(1,0)}$ to be the unique solution of (22) with first derivative equal to zero at the bottom, the general solution of (22) has the form

$$Z^{(1,0)} = Z_*^{(1,0)} + a_{10}Z. \quad (24)$$

The value of a_{10} can be chosen so that $B(x,t)$ is, to first-order in ϵ, the amplitude of the isopycnal displacement, the surface current, the bottom current, etc. Or one could choose a_{10} so that Z and $Z^{1,0)}$ are orthogonal. Similar comments apply to the $Z^{(0,1)}$ term. The appropriate choice for $B(x,t)$ is, of course, an issue even at leading order. Assuming wave amplitudes are nondimensionalized so that $\max B(x,t)$ is $O(1)$, the physical interpretation of B determines the value of ϵ for any comparison with a given physical situation. Whatever choice for B is made, the corresponding vertical structure should be scaled to have a maximum magnitude of 1.

As is well known, solitary wave solutions of the KdV equation exist of the form

$$B = a\text{sech}^2\left(\frac{x-Vt}{\lambda}\right), \quad (25)$$

where

$$V - c = \frac{4\mu\beta}{\lambda^2} = \frac{1}{3}\epsilon a\alpha. \quad (26)$$

The coefficients of the KdV equation are

$$I\,\alpha = 3\int (c-U)^2 Z'^3\,dy, \quad (27)$$

$$I\,\beta = \int (c-U)^2 Z^2\,dy, \quad (28)$$

where

$$I = 2\int (c-U)Z'^2\,dz. \quad (29)$$

The dispersive coefficient β is always positive whereas the nonlinear coefficient α can have either sign. Because $\beta > 0$, from (26) we see that $V > c$ and that α and a must have the same sign. Hence KdV solitary waves are waves of elevation/depression when α is positive/negative. From (26) we can also see that as the waves get larger (a increases) the waves become narrower (λ decreases). The KdV equation does not impose a limit to possible wave amplitudes. There is an implicit bound imposed by the requirement that the terms in the asymptotic expansions (11)–(13) are decreasing. Flat crested waves as depicted in Figure 1 are not possible within this theory.

For large waves, or for stratifications for which α is very small, it is necessary to include higher-order nonlinear effects by including terms of $O(\epsilon^2)$. This results in the Gardner equation

$$B_t + cB_x + \epsilon\alpha BB_x + \epsilon^2\alpha_1 B^2 B_x + \mu\beta B_{xxx} = 0. \quad (30)$$

The cubic nonlinear coefficient α_1 is given by

$$\begin{aligned} I\,\alpha_1 = -3\int\Big\{&\frac{4}{3}\alpha(c-U)Z'Z_y^{1,0} \\ &- 3(c-U)^2 Z'^2 Z_y^{1,0} + 2(c-U)^2 Z'^4 \\ &+ \frac{1}{3}\alpha^2 Z'^2 - \frac{5}{3}\alpha(c-U)Z'^3\Big\}\,dy. \end{aligned} \quad (31)$$

Like α, it can have either sign. Because of the non-uniqueness of $Z^{(1,0)}$, the cubic coefficient α_1 is not unique. It has the general form

$$\alpha_1 = \alpha_1^* + a_{10}\alpha, \quad (32)$$

where α_1^* is the value obtained when $Z^{(1,0)} = Z_*^{(1,0)}$. Varying the value of a_{10} can change the sign of α_1 unless $\alpha = 0$, in which case α_1. This means that in general there is no unique equation. How best to choose the appropriate wave amplitude and solution of the higher-order problems is still an open problem and probably depends on the stratification and background currents.

The Gardner equation has solitary wave solutions of the form

$$B = \frac{a}{b + (1-b)\cosh^2\theta} = \frac{a\text{sech}^2\theta}{1 - b + b\text{sech}^2\theta}, \quad (33)$$

where

$$\theta = \frac{x-Vt}{\lambda} \quad (34)$$

with

$$V - c = \frac{4\mu\beta}{\lambda^2} = \frac{\epsilon a}{3}\Big(\alpha + \frac{1}{2}\alpha_1\epsilon a\Big) \quad (35)$$

and

$$b = -\frac{\alpha_1\epsilon a}{2\alpha + \alpha_1\epsilon a}. \quad (36)$$

The requirement that B be finite restricts b to be less than 1. In addition, because $\beta > 0$, we must have

$$\alpha_1\epsilon a(\epsilon a + 2\alpha/\alpha_1) \geq 0. \quad (37)$$

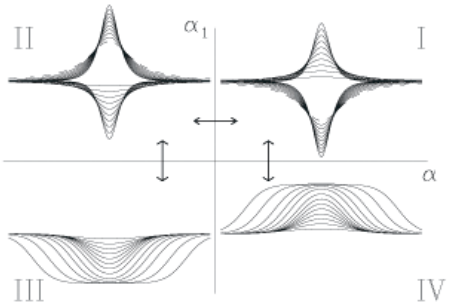

Figure 3. Schematic showing possible solitary wave solutions of the Gardner equation. The dashed lines indicate minimum wave amplitudes. Arrows indicate possible transitions of shoaling waves

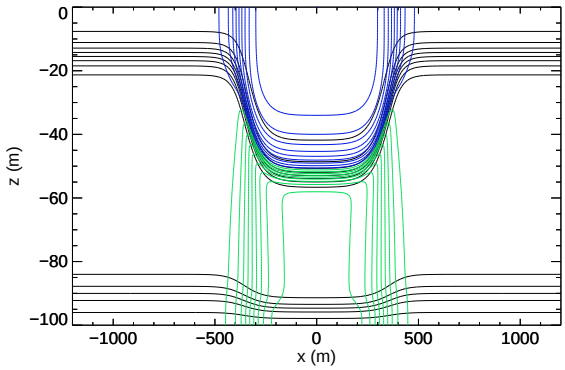

Figure 4. Exact ISW of depression in a continuous three-layer stratification. Black lines are density contours, blue/green are positive/negative horizontal velocity contours.

There are four cases, depending on the signs of α and α_1. These are illustrated in Figure (3) (idea from R. Grimshaw, E. Pelinovsky & T. Talipova). If $\alpha_1 < 0$, as the wave amplitude increases the wave amplitude increases at first and then the waves broaden as a limiting wave amplitude, given by

$$\epsilon a_{lim} = -2\frac{\alpha}{\alpha_1}, \tag{38}$$

is reached. The sign of the wave is determine by the sign of α.

If, on the other hand, $\alpha_1 > 0$ then waves of elevation and depression are both possible, irrespective of the sign of α. For one of the sets of waves, namely waves of elevation/depression for negative/positive α there is a minimum wave amplitude which is also given by (38). In these cases, solitary waves exist only if the waves are large enough that the cubic nonlinearity dominates the quadratic nonlinear term. When $\alpha_1 > 0$, there is no bound to the amplitudes of the waves, other than that implicitly imposed by the requirement that the asmptotic expansions (11)–(13) are well ordered.

The qualitative features of the limiting amplitudes can be seen by rewriting the Gardner equation as

$$B_t + \Big(c + \epsilon\alpha B + \epsilon^2\alpha_1 B^2\Big)B_x + \mu\beta B_{xxx} = 0. \tag{39}$$

If $\alpha_1 < 0$ then the coefficient of B_x, which is a nonlinear wave speed, becomes less than c regardless of the sign of α suggesting a limiting amplitude. If $\alpha_1 > 0$ then the coefficient of B_x is always larger than c if $\alpha B > 0$, suggesting waves of all amplitudes exist, and if $\alpha B < 0$ the coefficient of B_x is large than c if B is sufficiently large. Note that naively requiring that the coefficient of B_x is zero at the limiting amplitudes predicts a limiting amplitude equal to half that given by (38).

In the remaining sections we assume $\epsilon = \mu = 1$ with a suitable redefinition of the amplitude a and λ, or a rescaling of B and x.

Examples without background currents

Consider a couple of example stratifications. The first is a two layer fluid with upper and lower layer depths h_1 and h_2. This is a model for a stratification with a single thin pycnocline separating two homogeneous layers. For this stratification

$$c^2 = \frac{g'h_1h_2}{h_1+h_2}, \tag{40}$$

$$\beta = c\frac{h_1h_2}{6} \tag{41}$$

$$\alpha = \frac{3c}{2}\frac{h_1-h_2}{h_1h_2}, \tag{42}$$

$$\alpha_1 = -\frac{3c}{8h_1^2h_2^1}\Big(h_1^2+h_2^2+6h_1h_2\Big). \tag{43}$$

Here, the solution is fixed by fixing B to be the interface displacement. Note that α_1 is always negative, so only cases III and IV (Figure 3) are possible. The limiting amplitude of solitary waves is

$$a_{\text{lim}} = -\frac{\alpha}{\alpha_1} = 4\frac{(1-2h_2)(1-h_2)h_2}{1+4h_2-4h_2^2} \tag{44}$$

assuming $h_1 + h_2 = 1$. The limiting amplitude of exact fully nonlinear waves can be computed (*Amick and Turner* 1986; *Lamb* 2000). A comparison of the two predictions is shown in Figure 4. The weakly nonlinear prediction is a good approximation only if the limiting amplitude is less than approximately a quarter of the total depth.

The second model stratification considered is one for which α_1 can be positive. The simplest such stratification

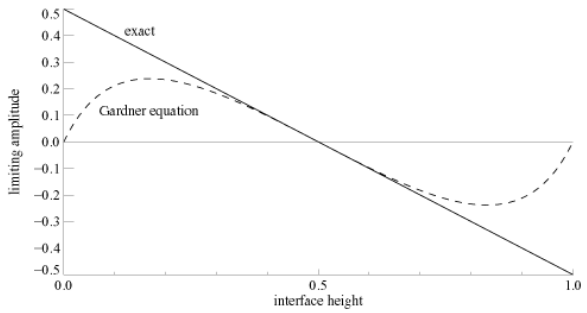

Figure 5. Limiting wave amplitudes predicted by Gardner equation and by fully nonlinear theory.

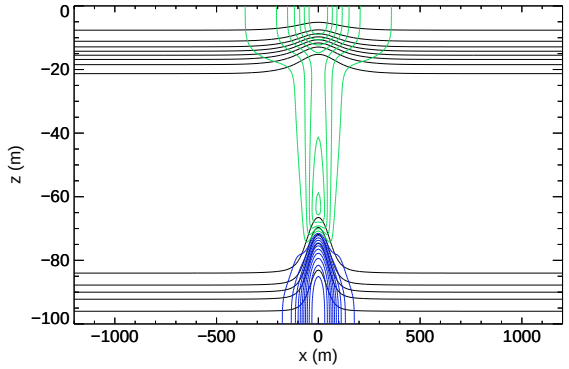

Figure 6. Exact ISW of elevation in a continuous three-layer stratification. Contour lines as in Figure 5.

is a 3-layer symmetric stratification with upper and lower layers of equal thickness h and the same density jump at each interface. Then, by symmetry $\alpha = 0$ for mode-1 waves which means that α_1 is uniquely determined. *Talipova et al.* (1999) found that the cubic nonlinear coefficient is

$$\alpha_1 = -\frac{3c}{4h^2}\left(13 - \frac{9H}{2h}\right), \tag{45}$$

which is positive if

$$h < 9H/26 = 0.346H. \tag{46}$$

Because $\alpha = 0$, this implies that there are no ISWs if $h > 9H/26$ but that ISWs of either sign, with no minimum or maximum amplitude, can exist if $h < 9H/26$, i.e., if the two interfaces are sufficiently close to the upper and lower boundary.

The qualitative predictions of the Gardner equation are qualitatively borne out by calculations of exact fully nonlinear waves, other than the lack of a limiting amplitude when $\alpha_1 > 0$. For example, consider the stratification

$$\bar{\rho}(z) = 1 - 0.005\tanh\left(\frac{z+15}{5}\right) - 0.003\tanh\left(\frac{z+90}{5}\right). \tag{47}$$

where $-100 \le z \le 0$. This continuous three-layer stratification has waves of depression which become flat-crested (i.e., conjugate flow limited) as shown in Figure 5, along with waves of elevation (Figure 6).

Next, consider a two-parameter family of continuous stratification, which approximate three-layer stratifications, given by

$$\bar{\rho}(z) = 1 - 0.005\left(\tanh\frac{z-z_1}{0.0556} + \tanh\frac{z-z_2}{0.0556}\right). \tag{48}$$

for $-1 < z < 0$. When $z_1 + z_2 = -1$ we recover a continuous approximation of the symmetric stratification considered by *Talipova et al.* (1997). A summary of the results of some calculations of fully nonlinear ISWs is presented in Figure 7. Here the grey shaded region indicates (z_1, z_2) values for which $\alpha > 0$. In this regions KdV theory predicts waves of elevation only. In the white regions $\alpha < 0$ in which case ISWs of depression are predicted. Along the diagonal $z_1 = z_2$ the two pycnoclines coincide. This corresponds to a two-layer fluid. When the pycnoclines are in the upper/lower half of the water column ISWs are waves of depression/elevation.

Along the other diagonal, $z_1 + z_2 = -1$, the stratification is symmetric and the quadratic nonlinear coefficient is equal to zero. There are two other zero contours. To understand their existence consider the vertical line $z_1 = 0$. As $-z_2$ increases from zero ISWs waves are waves of depression at first until the lower pycnocline moves into the lower half of the water column. The ISWs become waves of elevation when $-z_2 > 0.5$ because the lower pycnocline dominates. The upper pycnocline, which is centred at the top boundary, is not dynamically significant because its vertical displacements are constrained to be small by the presence of the boundary. As the upper pynocline moves down ($-z_1$ increases) the lower pycnocline must move further down to maintain waves of elevation. The zero contour passing through $(-z_1, -z_2) = (0, 0.5)$ terminates at $(0.5, 1.0)$. For a three layer fluid it can be shown that the intersection with the contour $z_1 + z_2 = -1$ is at $z_1 = 0.3$, i.e., at $h = 0.3H$ where $h = -z_1 = 1 + z_2$ is the thickness of the upper and lower layers. Note that the figure must by symmetric about $z_1 + z_2 = -1$.

Computations of exact ISWs showed that waves of either polarity are possible only above the $\alpha = 0$ contour joining $(-z_1, -z_2) = (0, 0.5)$ to $(-z_1, -z_2) = (0.5, 1)$ or below the $\alpha = 0$ contour joining $(-z_1, -z_2) = (0.5, 0)$ to $(-z_1, -z_2) = (1, 0.5)$. Thus, waves of either polarity along $z_1 + z_2 = -1$ are only possibly if $h = z_1 < 0.3$ instead of

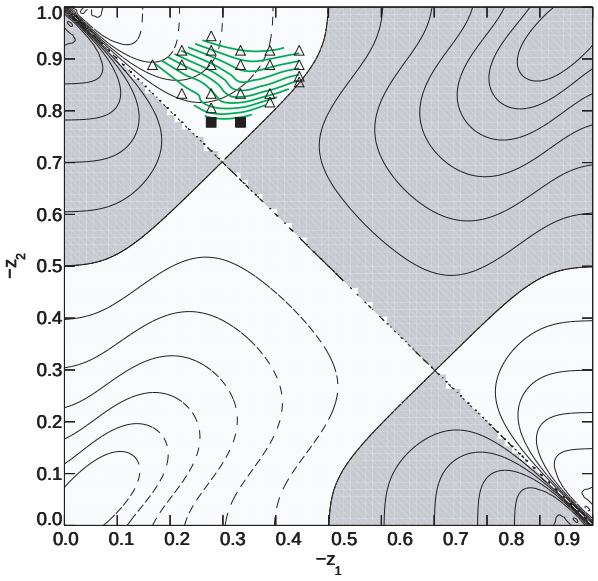

Figure 7. Exact ISW solutions for a continuous three-layer stratification. Black contour lines are contours of constant α, the shaded grey regions are regions where $\alpha > 0$ while the white regions have $\alpha < 0$. The open triangles: waves of elevation exist with a minimum amplitude greater than zero. Solid squares: waves of elevation with no minimum amplitude. Green contours are contours of minimum wave amplitudes equal to 0.02–0.2 in steps of 0.02.

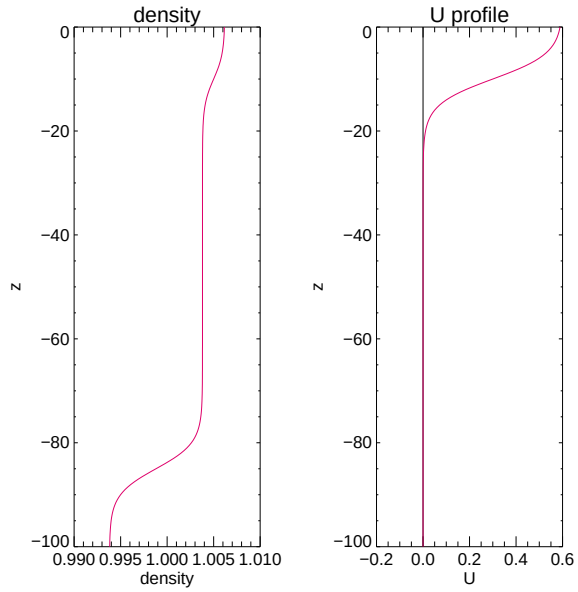

Figure 8. Background stratification and velocity.

0.346 as predicted by Talipova *et al.* (1997). The theoretically predicted critical value of h is about 15% too large.

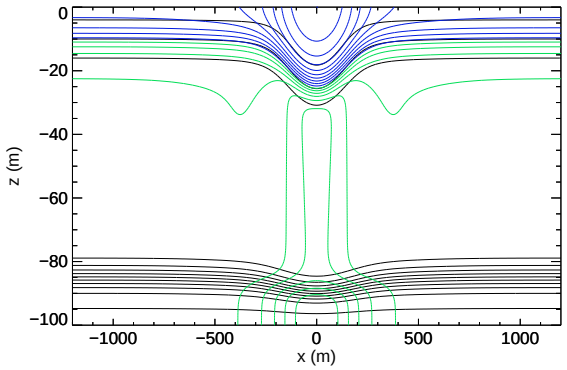

Figure 9. Exact internal solitary wave. Black lines are density contours, blue/green are positive/negative horizontal velocity contours.

Effect of Background Shear

Finally, we briefly consider a single example to illustrate the effects of a background velocity shear. The background density stratification and current are

$$\bar{\rho}(z) = 1 - 0.005 \tanh \frac{z+85}{5} - 0.00012 \tanh \frac{z+10}{5}, \tag{49}$$

$$U(z) = 0.3 \left(1 + \tanh \frac{z+10}{5} \right), \tag{50}$$

for $-100 \le z \le 0$, and are shown in Figure 8. The strongest stratification is near the bottom and, in the absense of a background current only ISWs of elevation exist. The presence of the background current with near surface shear enables the existence of ISWs of depression as shown in Figure 9. Note that the background shear has the same sign as the surface shear induced by a wave of depression.

A shoaling wave

To illustrate the formation of a wave train with waves of both polarities we consider a shoaling wave in a continuous three-layer stratification

$$\bar{\rho}(z) = 1 - 0.005 \tanh \left(\frac{z+5}{2} \right) - 0.01 \tanh \left(\frac{z+30}{4} \right), \tag{51}$$

which has been nondimensionalized by the density density at the surface. The water depth is

$$d(x) = 100 - 30(1 + \tanh(x/200)). \tag{52}$$

Both pycnoclines have the same maximum N the lower one is twice as thick and has double the density change across it. In the deep water (depth 100 m) both pycnoclines are in the

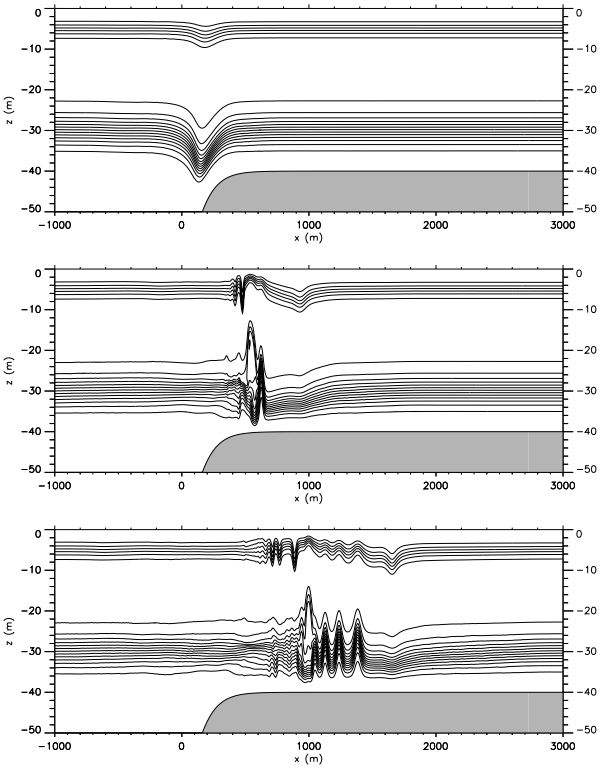

Figure 10. Density contours of a shoaling wave passing through a turning point in a three layer stratification. Waves are at times t=1600 s, 2400 s, and 3200 s. Only part of the computational domain is shown.

upper half of the water column and only solitary waves of depression exist. In the shallow water (depth 40 m) waves of either polarity are present. The lower pycnocline is now below the mid-depth and it dominates the upper one in the sense that it makes the quadratic nonlinear coefficient α to be positive. While propagating from deep to shallow water the wave passes through a turning point, defined as the location at which $\alpha = 0$. In terms of Figure 3, the transition is from region III to region I, although here we deal with fully nonlinear waves and not with solutions of the Gardner equation.

A nonlinear, nonhydrostatic model (*Lamb* 2002) was initialized with a single solitary wave of depression with an amplitude of 5.86 m centred at $x = -3000$. Figure 10 shows contour plots of the density field at three different times as the wave shoals. The initial wave passes through a turning point and is almost completely destroyed. Only a small solitary wave of depression survives, followed by a train of solitary waves of elevation which are emerging from a large mode-two like feature which formed at the back of the initial shoaling wave. At later times the number of solitary waves of elevation a solitary increases as more emerge from this feature. The solitary waves of elevation propagate more rapidly than the wave of depression. The transformation of a single wave of depression to a train of much narrower waves of elevation upon passage through a turning point is predicted by variable-coefficient KdV models (e.g., *Talipova et al.* 1997).

Conclusions

Extreme internal solitary waves have been discussed in an ideal setting. The use of numerical methods to compute exact, fully nonlinear waves has revealed much about the properties of large waves, yet the surface has only been scratched. Much remains to be learned about large internal solitary waves in more complicated stratifications and in the presence of background currents.

It should be borne in mind that many large internal solitary-like waves observed in the ocean may not be well approximated by these idealized, exact internal solitary waves. Most, large solitary-like waves are generated by tidal flow over topographic features such as sills and the shelf break. As the internal waves generated at these locations radiate away it takes time for internal solitary waves to emerge. The waves that do emerge will generally be propagating through a spatially varying environment and hence will be continually adjusting to their local conditions. These make it possible, particularly in the case of shoaling waves, for internal solitary-like waves to be much larger than exact fully nonlinear solitary waves can be.

Acknowledgments. This research was supported by a grant from the Natural Sciences and Engineering Research Council of

Canada.

References

Aigner, A., D. Broutman and R. Grimshaw (1999). Numerical simulations of internal solitary waves with vortex cores, *Fluid Dyn. Res., 25*, 315–333.

Akylas, T. R., and R. H. J. Grimshaw (1992). Solitary internal waves with oscillatory tails. *J. Fluid Mech., 242*, 279–298.

Amick, C. J., and R. E. L. Turner (1986). A global theory of internal solitary waves in two-fluid systems, *Trans. Am. Soc., 298*, 431–484.

Brown, D. J., and D. R. Christie (1998). Fully nonlinear solitary waves in continuously stratified incompressible boussinesq fluids, *Phys. Fluids, 10*, 2569–2586.

Clarke, R. H., R. K. Smith and D. G. Reid (1981). The Morning Glory of the Gulf of Carpentaria: An atmospheric undular bore, *Mon Wea. Rev., 109*, 1726–1750.

Cheung, T. K., and C. G. Little (1990). Meteorological tower, microbarograph array, and sodar observations of solitary-like waves in the nocturnal boundary layer, *J. Atmos. Sci., 47*, 2516–2536.

Craig, W., P. Guyenne, and H. Kalisch (1984). A new model for large amplitude long internal waves. *C. R. Mecanique, 332*, 525–530.

Davis, R. E., and A. Acrivos (1967). Solitary internal waves in deep water, *J. Fluid Mech., 29*, 593–607.

Derzho, O. G., and R. Grimshaw (1997). Solitary waves with a vortex core in a shallow layer of stratified fluid, *Phys. Fluids 9*, 3378–3385.

Grue, J., A. Jensen, P.-O. Rusås, J. K. Sveen (2000). Breaking and broadening of internal solitary waves, *J. Fluid Mech., 413*, 181–217.

Lafond, E. C., (1959). Slicks and temperature structure in the sea. Research Report 937, U. S. Navy Electronics Laboratory, San Diego.

Lamb, K. G. (2000). Conjugate flows for a three-layer fluid, *Phys. Fluids, 12*, 2169–2185.

Lamb, K. G., (2002). A numerical investigation of solitary internal waves with trapped cores formed via shoaling, *J. Fluid Mech., 451*, 109–144.

Lamb, K. G., (2003). Shoaling solitary internal waves: on a criterion for the formation of waves with trapped cores. *J. Fluid Mech., 478*, 81–100.

Lamb, K. G., and B. Wan (1998). Conjugate flows and flat solitary waves for a continuously stratified fluid, *Phys. Fluids, 10*, 2061–2079.

Lamb, K. G., and K. Wilkie (2004). Conjugate flows with trapped cores. *Phys. Fluids, 16*, 4685–4695.

Manasseh, R., C.-Y. Ching and H. J. S. Fernando (1998), The transition from density-driven to wave-dominated isolated flows, *J. Fluid Mech., 361*, 253.

Moum, J. N., D. M. Farmer, W. D. Smyth, L. Armi and S. Vagle (2003). Structure and generation of turbulence at interfaces strained by internal solitary waves propagating shoreward over the continental shelf, *J. Phys. Oceanogr., 33*, 2093-2112.

Orr, M. H., and P. C. Mignerey (2003). Nonlinear internal waves in the South China Sea: Observation of the conversion of depression internal waves to elevation internal waves, *J. Geophys. Res., 108(C3)*, 3064, doi:10.1029/2001JC001163.

Ostrovsky, L. A., and J. Grue (2003). Evolution equations for strongly nonlinear internal waves, *Phys. Fluids, 15*, 2934–2948.

Stastna, M., and K. G. Lamb (2002). Large fully nonlinear internal solitary waves: The effect of background current,' *Phys. Fluids 10*, 2897–2999.

Stanton, T. P., and L. A. Ostrovsky (1998). Observations of highly nonlinear internal solitons over the Continental Shelf, *Geophys. Res. Lett., 25*, 2695–2698.

Talipova, T. G., E. N. Pelinovsky, and R. Grimshaw (1997). Transformation of a soliton at a point of zero nonlinearity, *JETP Lett., 65*, 120–125.

Talipova, T. G., E. N. Pelinovsky, K. Lamb, R. Grimshaw, and P. Holloway (1999). Cubic nonlinearity effects in the propagation of intense internal waves, *Doklady Earth Sciences, 365*, 3–16.

Trevorrow, M. V., (1998). Observations of internal solitary waves near the Oregon coast with an inverted echo sounder, *J. Geophys. Res., 103(C4)*, 7671–7680.

Tung, K.-K., T. F. Chan and T. Kubota (1982). Large amplitude internal waves of permanent form, *Stud. Appl. Math., 66*, 1–44.

Turkington, B., A. Eydeland and S. Wang (1991). A computational method for solitary internal waves in a continuously stratified fluid, *Stud. Appl. Math., 85*, 93–127.

This preprint was prepared with AGU's LaTeX macros v4, with the extension package 'AGU^{++}' by P. W. Daly, version 1.6a from 1999/05/21.